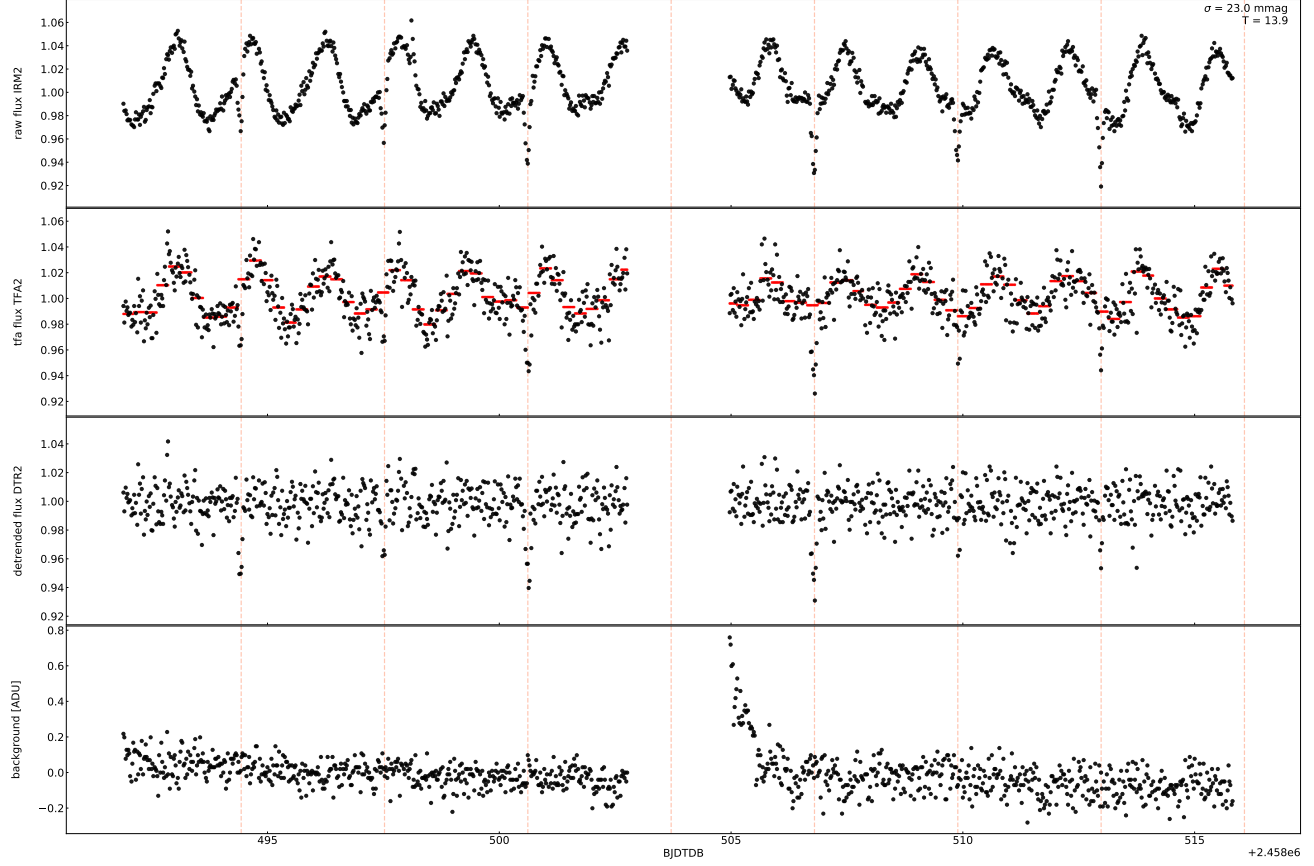
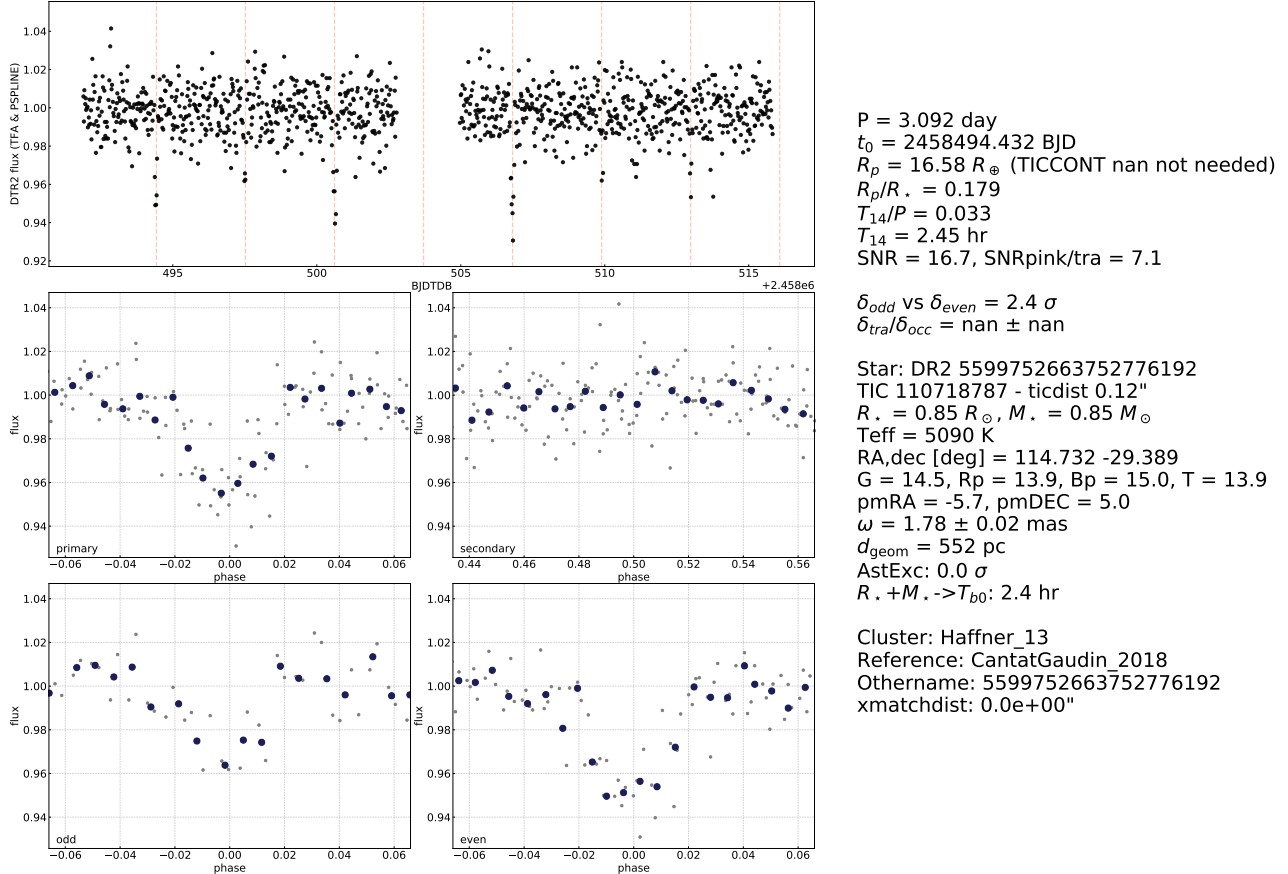


**Figure 19. Transit search summary.** Periodograms from TLS and phase-dispersion minimization, as calculated with `astrobase.periodbase`, are shown in the top left and top center (Bhatti et al. 2018; Hippke & Heller 2019; Stellingwerf 1978). The top three peaks from each method are shown in the second and third rows; the raw light curve is in the top-right. A small finder chart from DSS is inset to the top left, with the 1.5-pixel radius aperture used to extract the light curve in orange.



**Figure 20. Light curve diagnostics.** Time-series of raw flux (IRM2), TFA-detrended flux (TF2), stellar-variability detrended flux, and the background are shown as a function of barycentric Julian date. The overplotted dashed vertical lines are the ephemeris of the highest-power TLS peak from Figure 19. An important check is whether the flux dips are correlated with changes in the background level – in this case, they are not. The standard deviation and TESS magnitude are quoted in the upper right. The red line in the second from the top plot is the windowed spline described in Section 4.3, in this case an essential step for finding the eclipse signal.



**Figure 21. Transit diagnostics.** The plots show the maximally-detrended light curve (top); the phase-folded light curve centered over  $\pm 3$  transit durations of the primary transit (middle left); the secondary eclipse (middle right); the odd-numbered transits (lower left); and the even-numbered transits (lower right). The stellar parameters ( $T_{\text{eff}}$ ,  $R_\star$ ,  $M_\star$ ) are taken from TICv8 when available (Stassun et al. 2019). The first eight lines of text are parameters determined from the best-fitting TLS model. The one exception is the planet radius, which uses the stellar radius as noted above. The “flux contamination” (TICCONT) from neighboring stars is *never* taken into account, because transit depth dilution does not affect image subtraction analyses in the same manner as aperture-photometry reductions. The significance of the odd-to-even asymmetry is quoted, but given the strong rotational variability in this object (Figure 20), the apparent odd-even asymmetry could have been caused by the detrending process. To estimate the transit to occultation depth ratio  $\delta_{\text{tra}}/\delta_{\text{occ}}$ , the phase-folded light curve is also fit by a sum of two gaussians (in this case, the fit failed). “AstExc” refers to the Gaia-DR2 astrometric excess, which can indicate hints of astrometric binarity in the system. “ $d_{\text{geom}}$ ” is the geometric distance from Bailer-Jones et al. (2018). “ $R_\star + M_\star \rightarrow T_{b0}$ ” gives the duration of a zero-eccentricity central transit based on the TICv8 stellar radius and mass if available. If the mass is not available, a stellar mass is interpolated from the Pecaut & Mamajek (2013) table, under the assumption that the star is a dwarf.

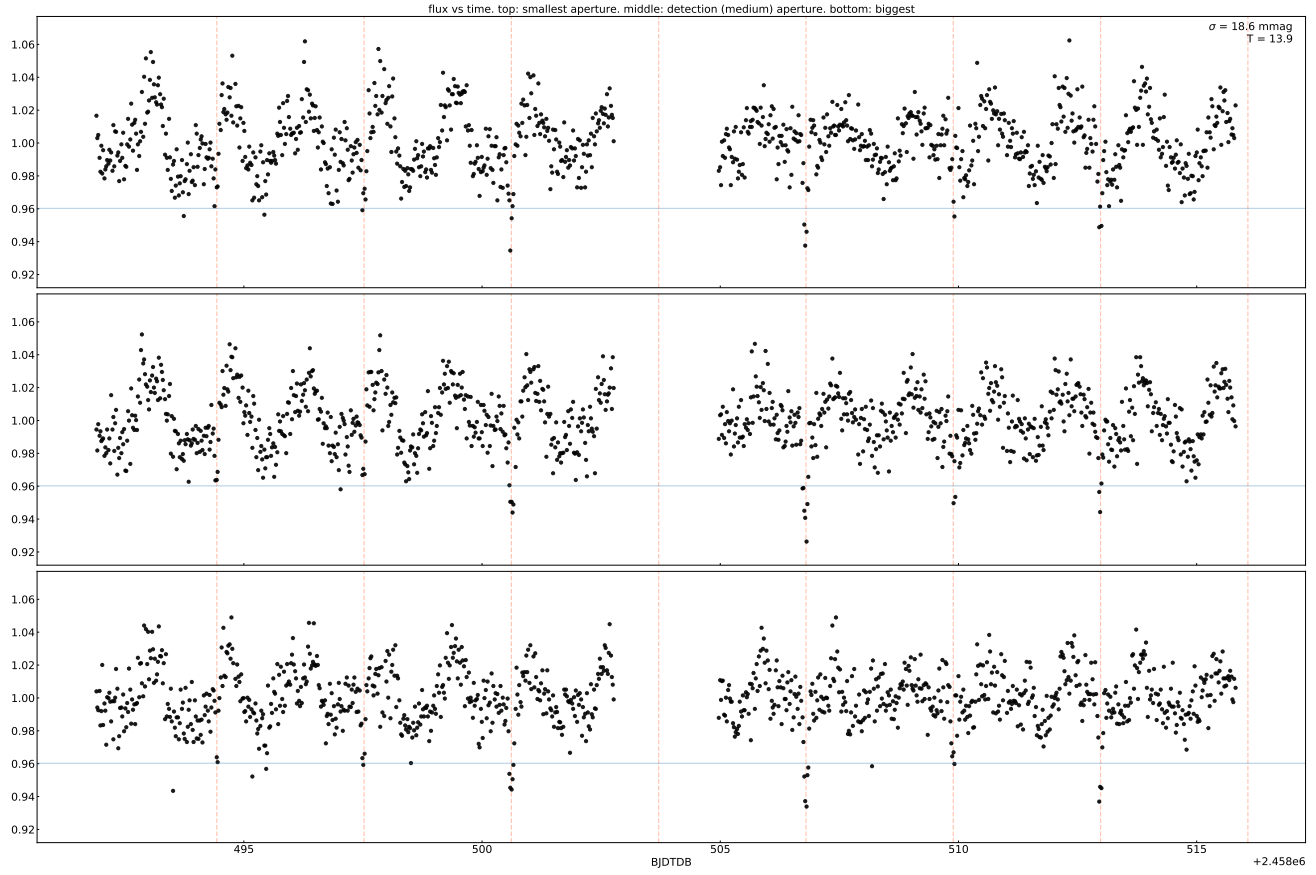
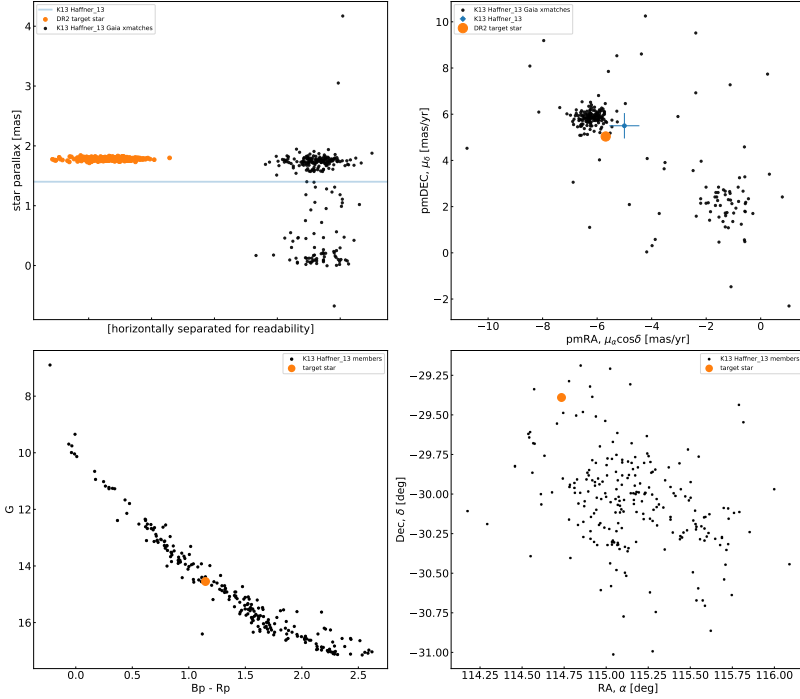


**Figure 22. Light curves for increasing aperture sizes.** Apertures of radius 1, 1.5, and 2.25 pixels are shown from top to bottom. The blue line is the reference transit depth from the best-fitting TLS model. Changes in depth with increasing aperture size can indicate that the source of variability is off-center from the aperture, suggesting a photometric blend.



Cluster: Haffner\_13  
 Reference: CantatGaudin\_2018  
 Starname: 5599752663752776192  
 xmatchdist: 0.0e+00"

K13 match: MWSC 1305, Haffner\_13  
 $N_{1sr2}$ : 126,  $\log t$  = 7.5,  
 type = oc,  $d_{K13}$  = 714 pc  
 Expect  $\omega_{K13}$  = 1.40 mas  
 Got  $\omega_{DR2}$  =  $1.78 \pm 0.02$  mas

Star: DR2 5599752663752776192  
 $R_* = 0.85 R_\odot, M_* = 0.85 M_\odot$   
 Teff = 5090 K  
 RA = 114.732, DEC = -29.389  
 G = 14.5, Rp = 13.9, Bp = 15.0  
 pmRA = -5.7, pmDEC = 5.0  
 $\omega = 1.78 \pm 0.02$  mas  
 $d = 1/\omega_{as} = 561$  pc

K13Note: Sparse; poor RDP.

**Figure 23. Cluster membership assessment diagnostics.** The star was considered a candidate cluster member by the source(s) listed under “Reference”, in this case [Cantat-Gaudin et al. \(2018\)](#). The name used in their catalog in this case was 5599752663752776192, a Gaia-DR2 identifier, which can be back-referenced to find that [Cantat-Gaudin et al. \(2018\)](#) assigned this star a membership probability in Haffner 13 of just 10%. The base catalog for the plots is chiefly that of [Kharchenko et al. \(2013\)](#), due to its homogeneous parameter determination procedure (particularly for age). If a match to the [Kharchenko et al. \(2013\)](#) catalog is found, then the remaining plots are populated. Top-left shows the parallax, with orange points sampled from the Gaia-DR2 posterior, black points the other cluster members in the Kharchenko catalog, and the blue line the claimed Kharchenko parallax for the cluster. A number of field contaminants in the Kharchenko catalog are visible in this case. Top-right are the Gaia proper motions, where against black points are cluster members from Kharchenko, and the orange is the target star. Bottom-left is the color-magnitude diagram, and bottom-right are the on-sky positions. In the text,  $N_{1sr2}$  is the number of  $1\sigma$  cluster members reported by [Kharchenko et al. \(2013\)](#) within the cluster angular radius;  $\log t$  is the base-10 logarithm of the age in years; type matches the type codes provided by [Kharchenko et al. \(2013\)](#); K13Note gives the description of the cluster from [Kharchenko et al. \(2013\)](#), if available. Extra caution must be taken when interpreting this set of plots, since they can only show disagreement between the observed star’s properties and those of the listed Kharchenko members (and the latter may be biased).

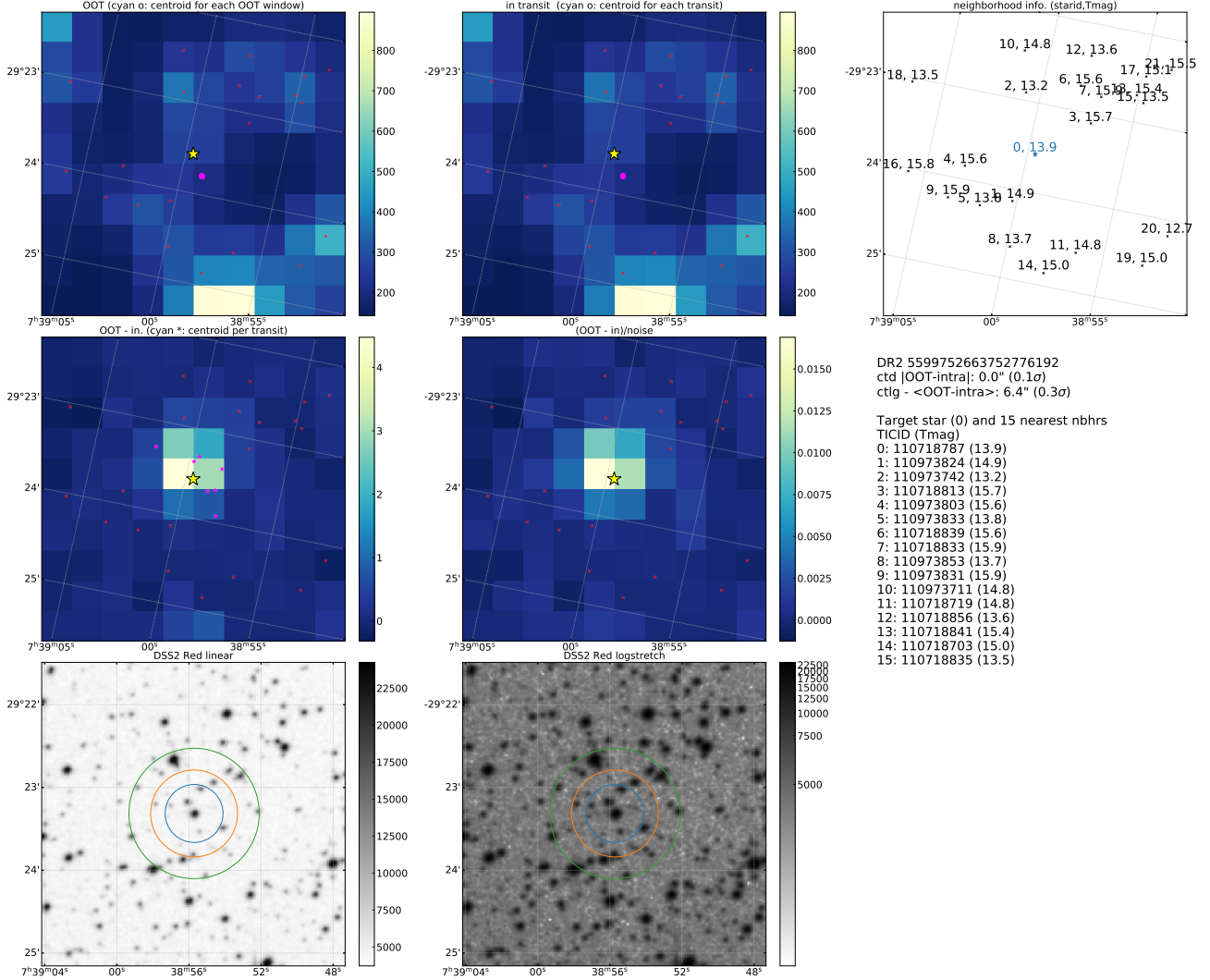


**Figure 24. Imaging variability diagnostics.** This page is intended to help diagnose which stars are producing the observed variability. Top-left and top-center are the mean out-of-transit (OOT) and mean in-transit calibrated images (separate from any of our image-subtraction analysis). The OOT images are based on the same number of exposures as the in-transit images and split evenly before and after each transit (following Bryson et al. 2013; Kostov et al. 2019). The yellow star is the target; cyan dots are the flux-weighted centroid of the entire image for each transit event; small red crosses are WCS-projected locations of neighbor stars. Middle-left is the most important sub-panel: the difference between the OOT and in-transit mean images. If the variability shown in background map (units: ADU) is off-target, the transit is typically not from the target star. Middle-center is the same, normalized by the uncertainty map. Lower left and lower center show the DSS field in linear and log scales at roughly the same pixel scale as the TESS image, with the 1, 1.5, and 2.25 pixel-radius apertures in blue, orange, and green respectively. The brightness of neighborhood stars is given on the far right. Note the slight coordinate rotation difference between DSS and TESS images; DSS images are aligned north-up, east-left; TESS images are oriented as closely as possible to this system without actually performing the rotation.